Calibration of matrix-dependent biases in isotope and trace element analyses of carbonate minerals

Kaitlyn A. McCain 🆔 , Ming-Chang Liu, and Kevin D. McKeegan

COLLECTIONS

Paper published as part of the special topic on Special Topic Collection on Secondary Ion Mass Spectrometry (SIMS)
Note: This paper is part of the 2020 Special Topic Collection on Secondary Ion Mass Spectrometry, SIMS.

View Online   Export Citation   CrossMark

ARTICLES YOU MAY BE INTERESTED IN

Development of two-color resonant ionization sputtered neutral mass spectrometry and microarea imaging for Sr
Journal of Vacuum Science & Technology B **38**, 044001 (2020); https://doi.org/10.1116/6.0000006

Analysis of useful ion yield for Si in GaN by secondary ion mass spectrometry
Journal of Vacuum Science & Technology B **38**, 044002 (2020); https://doi.org/10.1116/6.0000138

Self-detached membranes with well-defined pore size, shape and distribution fabricated by underexposure photolithography
Journal of Vacuum Science & Technology B **38**, 042601 (2020); https://doi.org/10.1116/6.0000203

Calibration of matrix-dependent biases in isotope and trace element analyses of carbonate minerals

Kaitlyn A. McCain,[a] 🔾 Ming-Chang Liu, and Kevin D. McKeegan

AFFILIATIONS

Department of Earth, Planetary, and Space Sciences, University of California at Los Angeles, 595 Charles E. Young Drive East, Los Angeles, California 90095

Note: This paper is part of the 2020 Special Topic Collection on Secondary Ion Mass Spectrometry, SIMS.
[a]**Electronic mail:** kamccain@ucla.edu

ABSTRACT

The timing of important events in the early history of the solar system can be established by using the decay of the short-lived radionuclide ^{53}Mn to stable ^{53}Cr. Carbonate minerals found in meteorite samples can be dated using this system provided that an accurate and precise value for the Mn/Cr ratio can be established. However, the ion yields of Mn and Cr vary substantially based upon the elemental composition of the matrix and require calibration using standards of known Mn and Cr concentrations to relate the measured Mn/Cr ratio to the true ratio with a "relative sensitivity factor." The authors implant ^{52}Cr^{+} into a suite of terrestrial calcite and dolomite samples of varied elemental compositions to produce matrix-matched standards for ^{53}Mn-^{53}Cr analysis. Depth profiling of the implanted carbonates reveals variation in the relative sensitivity factors between carbonates low in Fe and Mn and dolomite rich in Fe and Mn. For carbonates with $FeCO_3 > 8$ mol. %, the relative sensitivity factor is constant at 0.88 ± 0.08 (2SD). For carbonates with $FeCO_3 < 2$ mol. %, the relative sensitivity factor is approximately 1.1. The authors also show that the use of an inappropriate relative sensitivity factor can lead to systematic errors in the age determined for meteoritic carbonate.

Published under license by AVS. https://doi.org/10.1116/6.0000111

I. INTRODUCTION

The determination of a chronology of key events in the chemical and mineralogical evolution of planetary materials is critical to developing a detailed understanding of processes associated with the formation of the solar system. Such significant events include the accretion times of asteroids and the timing of important thermal processing events (e.g., circulation of hydrothermal fluids). Early solar system materials are found in primitive meteorites ("chondrites") and specific mineral phases can be dated with high precision using a variety of short-lived radiometric systems.[1] One such system is based on the radioactive decay of ^{53}Mn to ^{53}Cr with a half-life of 3.7 Myr. The relatively high abundance of ^{53}Mn in the early solar system and its short half-life allows a mineral which incorporated this nuclide within the first ~15 Myr of the birth of the solar system to have its relative age determined with good precision, in ideal circumstances at submillionyear levels.

Solar system materials that have experienced alteration by aqueous fluids are of special interest to the planetary science community because liquid water makes possible complex organic and inorganic chemistries, even on small planetary bodies like asteroids. The secondary minerals formed by this alteration can be dated to determine the age and longevity of these water-rich environments. One useful group of minerals are carbonates, which form only in water-rich environments and preferentially incorporate 2+ ions (e.g., Ca, Mg, Fe, and Mn) and exclude 3+ ions (such as Cr) during crystallization. Carbonates forming early in the history of the solar system had the potential to incorporate radioactive ^{53}Mn, which would have subsequently decayed to ^{53}Cr, leaving a "fossil" record of its former presence as an elevated ^{53}Cr/^{52}Cr ratio correlated to Mn abundance. The relative age of the carbonate can be estimated by comparing its inferred initial ^{53}Mn/^{55}Mn ratio with that of an "anchor" sample of the known age, assuming ^{53}Mn was homogeneously distributed in the early solar system.[1] This anchor sample is a differentiated meteorite whose ^{53}Mn/^{55}Mn has been determined to be 3.24×10^{-6} at 4563.4 Myr before present.[2,3] As shown in Eq. (1), the formation age of the carbonate in millions of years before present ($T_{carbonate}$)

may be calculated based on the inferred isotopic composition of Mn incorporated into the carbonate mineral $(^{53}\text{Mn}/^{55}\text{Mn})_{\text{carbonate}}$,

$$T_{\text{carbonate}} = 4563.4 + \frac{t_{1/2}}{\ln(2)} \times \ln\left[\frac{(^{53}\text{Mn}/^{55}\text{Mn})_{\text{carbonate}}}{3.24 \times 10^{-6}}\right]. \quad (1)$$

Because ^{53}Mn has undergone over one thousand half-lives since the formation of the carbonates, it can be considered to have decayed completely and the present day $^{53}\text{Mn}/^{55}\text{Mn}$ ratio cannot be directly measured in meteoritic carbonate. However, Cr was strongly excluded from the mineral during its formation, and so ^{53}Cr detected in meteoritic carbonates can be attributed to the decay of ^{53}Mn. Therefore, it is possible to infer the initial $^{53}\text{Mn}/^{55}\text{Mn}$ ratio in a carbonate by determining the amount of radiogenic ^{53}Cr present. This is done by observing the correlation of $^{53}\text{Cr}/^{52}\text{Cr}$ with the parent-element/daughter-element ratio, $^{55}\text{Mn}/^{52}\text{Cr}$. Previous analyses of meteoritic carbonate using this system suggest that most carbonates formed 3–7 Myr after the birth of the solar system.[4–8]

Meteoritic carbonates are small, difficult to separate from the host meteorite, and texturally complex. Therefore, most meteoritic carbonate is dated *in situ* using secondary ion mass spectrometry (SIMS or ion probe), allowing both Mn and Cr species to be sampled from identical volumes in individual grains. To infer the correct formation age of a carbonate requires that the Mn/Cr ratio be determined accurately and precisely, but elemental ratios are difficult to measure by ion probes, as the ion yields of different elements often vary substantially based upon the elemental composition of the matrix, a phenomenon known as the "matrix effect." The magnitude of this effect is difficult to model and must be corrected empirically by measuring standards of similar chemical composition and known Mn/Cr ratio (i.e., "matrix-matched"). Carbonates, in particular, exhibit strong matrix effects related to the abundance of Fe in the target carbonate.[8]

In order to obtain accurate elemental ratios, it is necessary to relate the true concentrations of each element (C_a and C_b) to the intensities (I_a and I_b) measured by the ion probe via a relative sensitivity factor, or "RSF," shown in Eq. (2),

$$\text{RSF} = \frac{C_a/C_b}{I_a/I_b}. \quad (2)$$

Reference materials (or "standards") can be analyzed to determine an RSF provided that the concentrations of the target elements are known and homogeneously distributed. In the case of carbonate minerals, however, such reference materials for the Mn/Cr ratio cannot be found in nature due to the strong exclusion of 3+ ions such as Cr from the carbonate crystal structure, and synthetic materials face challenges associated with growing homogeneous Cr-doped calcite[7,9] and synthesizing dolomite.[10] Because matrix-matched reference materials of the known Mn/Cr ratio are not easily acquired or made, previous studies of meteoritic carbonate were restricted to using RSF values determined on materials of known Mn/Cr ratios which did not closely match the chemistry of the target carbonate minerals (and thus could be subject to matrix effects).

As an alternative to unaltered naturally occurring or synthetic RSF reference materials, ion accelerators can be used to implant Cr into natural minerals with excellent lateral spatial homogeneity.[11] This technique allows any implanted material to become a standard of known Cr concentration so long as the total amount of implanted ions, or fluence, can be determined following correction for any initial Cr present. In a study where a variety of carbonate minerals were implanted with $^{52}\text{Cr}^+$, the RSF between Mn and Cr was shown to vary significantly as a function of the Fe and Mn contents of the mineral.[8]

Previously implanted materials have been used to constrain the RSF for a large chemical range of carbonates.[8] However, most carbonates appropriate for Mn-Cr dating in meteorites are dolomites containing up to $\sim$20 mol. % Fe. Only two carbonates implanted previously are within this range of natural meteoritic carbonate, dolomites with 25 and 9 mol. % Fe (replacing Mg). The variation of the RSF in carbonate minerals relevant to studies of meteorite ages, i.e., the full range of matrix effects, is not yet determined. In this work, we measured the RSF of calcite and dolomite minerals with Fe contents ranging over 0–20 mol. % in order to improve the accuracy of radiometric dating of carbonate in meteorites.

II. EXPERIMENT

A. Sample selection and preparation

Natural carbonate minerals were selected from the UCLA mineral collection, including calcite (CaCO_3), Fe-poor dolomite [$\text{CaMg(CO}_3)_2$], and Fe-rich ferroan dolomite [$\text{Ca(Mg,Fe)(CO}_3)_2$]. The minerals span the range of Fe contents observed in meteoritic carbonate, between 0 and 20 mol. % FeCO_3. A comparison of carbonate minerals in our study, meteoritic carbonate, and previously implanted carbonates can be found in the supplementary material.[20] A large crystal fragment of each mineral was embedded in Field's Metal and/or indium in the center of an aluminum disk, and polished to better than $0.25\,\mu\text{m}$ using a Beuhler MetaDi Supreme polycrystalline diamond compound. Samples of NIST 612 and NIST 614 soda lime glasses, which are certified concentration reference materials containing 36 ppm and 1 ppm Cr and 39 ppm and 1.3 ppm Mn, respectively,[12] were also mounted to be used to calibrate the implant fluence.

B. Electron probe microanalysis

The chemical composition and homogeneity of each mineral was determined using the JEOL Superprobe electron microprobe analyzer (EPMA) at UCLA using an accelerating voltage of 15 kV with a beam defocused to $10\,\mu\text{m}$ to avoid damage to the carbonate minerals. Full details of the EPMA analytical conditions can be found in the section "Supplementary Methods" of the supplementary material.[20] In all cases, Cr concentrations in these natural carbonates were below the detection limit of the EPMA ($\sim$120 ppm). Carbonate minerals with homogeneous Fe content—that is, minerals for which repeated analyses remained within 2SD (internal error) of one another—were selected for depth profiling. The mounted fragment of the ferroan dolomite MS1312 was found to have two domains with distinct Fe and Mn concentrations, and

these domains were treated separately. The composition of each selected carbonate mineral is summarized in Table I, with the two domains of MS 1312 reported as MS 1312_D1 and MS1312_D2 referring to the high and low Mn domains, respectively.

C. Ion implantation

The mount was coated with a 30 nm layer of gold to ensure conductivity and prevent charging during ion implantation and ion probe analysis. The mount was implanted with a 185 KeV $^{52}Cr^+$ ion beam at a nominal fluence of 4×10^{13} ions/cm^2, rastered over the entire surface. A mass filter was used to separate $^{52}Cr^+$ and $^{53}Cr^+$ after Cr ionization, ensuring that only $^{52}Cr^+$ was implanted. If some amount of $^{53}Cr^+$ was included during implantation, the $^{53}Cr^+$ abundance observed during depth profiling would increase and then decay similarly (though at lower abundance) to $^{52}Cr^+$, which was not observed in any of our implanted materials. The implantation was carried out by Leonard Kroko, Inc.

1. Modeling of backscatter effects during implantation

Variation in the chemistry of implanted targets can impact the total quantity and distribution of implanted ions within the target material. In particular, a target containing a higher proportion of high-Z elements such as Fe will backscatter the incident ion beam more efficiently than a target with fewer high-Z elements. If backscatter effects are sufficiently strong, dolomite samples with higher Fe contents could receive a lower dose of $^{52}Cr^+$ ions than targets with low Fe.

To constrain the magnitude of the backscatter effect in our implanted minerals, we used the SRIM (Stopping Range of Ions in Matter) program to simulate a dose of 2000 $^{52}Cr^+$ ions with an energy of 185 keV into soda lime glass, pure $CaCO_3$, $CaMgCO_3$, $Ca(Mg_{0.75},Fe_{0.25})(CO_3)_2$, and $Ca(Mg_{0.5},Fe_{0.5})(CO_3)_2$, all with a 30 nm Au coating.[13] Four replicate simulations were performed for each target material. For all targets, including the NIST glasses, approximately $10 \pm 0.5\%$ of incident $^{52}Cr^+$ ions were backscattered by the gold coat, with no correlation between the number of backscattered ions and Fe content. Because all targets showed identical

backscattering behavior, we conclude that all targets received the same fluence, and, therefore, we do not apply separate backscatter corrections to our fluence calculations.

The distribution of the simulated implanted $^{52}Cr^+$ did not vary significantly between the dolomite targets, with the peak implanted Cr concentration occurring at approximately 92 nm for all simulated dolomites. The simulated peak concentration for the glass target occurred deeper within the material at 108 nm. We suspect that this difference arises from the glass's lower density compared to dolomite minerals. Additional documentation of the SRIM simulations can be found in the supplementary material.[20]

D. Depth profiling

The implanted carbonate standards and NIST standard materials were analyzed on the Cameca ims-1290 ion microprobe at UCLA equipped with an Oregon Physics Hyperion oxygen plasma source. Two separate areas of each target material were analyzed by sputtering with a 2 nA O^{3-} primary ion beam focused into a $\sim 3\,\mu m$ spot rastered over $\sim 50\,\mu m$ by $\sim 50\,\mu m$ areas in each implanted material. A field aperture was inserted into an ion image plane to restrict the collected ions to the central $20\,\mu m$ by $20\,\mu m$ area of each raster square. A $75\,\mu m$ entrance slit was used. Secondary ions of $^{44}Ca^+$, $^{52}Cr^+$, $^{53}Cr^+$, and $^{55}Mn^+$ were counted using an electron multiplier. The profile MS1317J No. 2 was acquired by sputtering for over twice as long to test whether the signal varied with increasing depth. For the ferroan dolomite MS1312, the two depth profiles were placed in the two different compositional regions: The profile "MS1312 No. 1" was collected from the higher-Mn domain (MS1312_D1), and the profile "MS1312 No. 2" from the lower-Mn domain (MS1312_D2).

Each material was sputtered until the $^{52}Cr^+$ and $^{53}Cr^+$ signals decayed to a stable background, which occurred in approximately 30 min. Representative profiles of the intensities as collected from NIST glass NBS 614 and the natural carbonate MS1317J are shown in Figs. 1 and 2, respectively. The maximum implanted ^{52}Cr concentration depth is deeper in the NIST 614 glass, and the implant profile decays to background more slowly than in the MS1317J dolomite, which we attribute to the effect of mineral density identified during our SRIM modeling. Additional profiles for all sputtered materials are included in the supplementary material.[20]

To get the implantation profile of ^{52}Cr, the measured $^{52}Cr^+$ signal was corrected for the natural abundance of ^{52}Cr in the mineral, which is calculated by multiplying the $^{53}Cr^+$ signal by the terrestrial $^{52}Cr/^{53}Cr$ ratio of 8.8190. The corrected $^{52}Cr^+$ signal was calculated at every block using the $^{53}Cr^+$ intensity recorded in the same block. This dynamic correction was necessary as the abundance of both Cr isotopes varied with depth over the time of the profile. Besides the variation in ^{52}Cr abundance attributed to the ion implantation procedure, background ^{52}Cr and ^{53}Cr are typically elevated at the beginning of the profile due to surface contamination.

E. Surface profilometry

The depth of each ion beam raster square was measured using the Dektak XT stylus profilometer at the Molecular

TABLE I. Summary of elemental composition of carbonate minerals determined by electron probe microanalysis. Concentrations are reported in molar percent except when concentrations of Mn are reported in ppm as μg Mn/g. Errors are reported as 2SD mol. % and incorporate the internal variation during analysis and the SD of repeated analyses. The detection limit of Fe and Mn is approximately 120 ppm, and elements below the detection limit are marked "b.d." Compositions marked with an asterisk denote material compositions determined by a higher current beam following depth profiling analysis [see supplementary material (Ref. 20)].

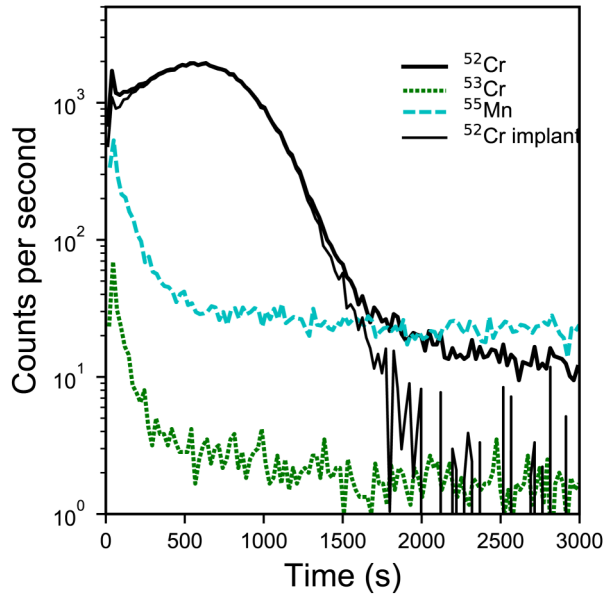| Name	Ca	±	Mg	±	Fe	±	Mn	±
Calcite	99.4	0.8	0.5	0.2	b.d.	–	b.d.	–
MS1317*	50.1	0.4	49.8	0.4	b.d.	–	(317)	(203)
MS1317J*	50.2	0.3	48.2	0.3	1.4	0.1	0.2	0.04
MS1318	48.0	0.5	42.7	0.3	8.2	0.2	1.1	0.2
MS1305*	49.5	0.3	49.4	0.4	0.9	0.1	(558)	(270)
MS1312_D1*	50.1	0.3	18.8	0.7	22.8	1.0	8.2	0.3
MS1312_D2*	49.6	0.4	21.8	0.7	21.9	0.9	6.6	0.2

FIG. 1. Intensities of $^{52}Cr^+$, $^{53}Cr^+$, and $^{55}Mn^+$ recorded during depth profiling of NIST 614 glass. The heavy black line represents the intensity of $^{52}Cr^+$ including the implanted Cr and the background Cr in the NIST glass. The dotted green line represents the intensity of the background $^{53}Cr^+$ during the profile. The dashed blue line represents the intensity of $^{55}Mn^+$ during the profile. The thin black line represents the intensity of $^{52}Cr^+$ attributed to ion implantation.

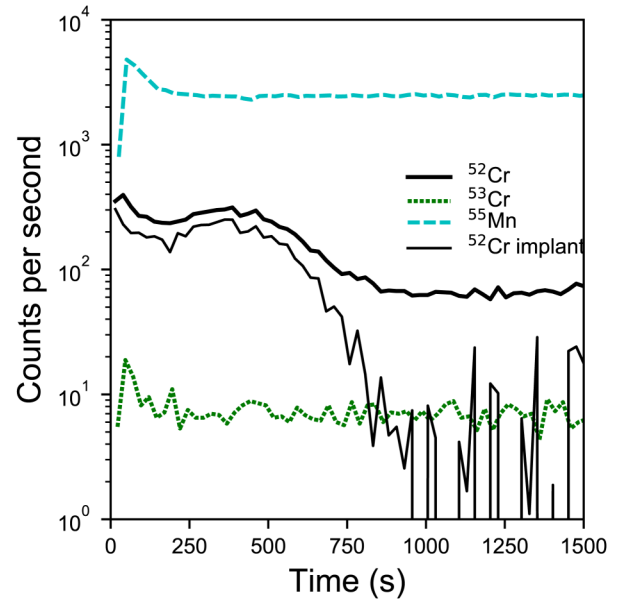**FIG. 2.** Intensities of $^{52}Cr^+$, $^{53}Cr^+$, and $^{55}Mn^+$ recorded during depth profiling of the natural dolomite MS 1317J No. 2. The heavy black line represents the intensity of $^{52}Cr^+$ including the implanted $^{52}Cr^+$ and the background Cr in the dolomite. The dotted green line represents the intensity of the background $^{53}Cr^+$. The dashed blue line represents the intensity of $^{55}Mn^+$. The thin black line represents the intensity of ^{52}Cr attributed to ion implantation.

Materials Research Center at the California Institute of Technology. Profiles were collected using a stylus tip diameter of $2\,\mu m$, a vertical range of $6\,\mu m$, and a vertical resolution of 0.1 nm. Each raster was profiled two times along perpendicular axes. The depth of each profile was determined using the Bruker Vision64 software, which determines the vertical distance between the flat region surrounding the rastered area and the flat bottom of the profile, which trims the edges of the rastered area from the depth. The rastered areas were flat and did not show significant curvature at their bottoms. The average value of the depth of the two profiles was taken as the depth of the rastered area. The depth of each profile is summarized in Table II, and additional information including SEM imagery of the rastered areas can be found in the supplementary material.[20]

III. RESULTS AND DISCUSSION

A. Calibration of implant fluence

While ion implantation guarantees a laterally homogeneous concentration of the implanted species, the accuracy of the fluence delivered can only be guaranteed to 10%–20% of the nominal requested fluence. It is therefore necessary to independently calibrate the $^{52}Cr^+$ fluence received using materials with known (and homogeneous) Cr concentration. In this case, the two co-implanted NIST glasses described above were used to calibrate the implant fluence as previously described by Steele *et al.*[8] in Eq. (3), where

F_{52Cr} refers to the actual fluence of the implanted ^{52}Cr, C_{52Cr} refers to the true concentration of ^{52}Cr as certified by NIST, and D refers to the depth of the analysis crater. A_{52Cr+} refers to the sum of all $^{52}Cr^+$ counts attributed to the implant, corrected for the background concentration of ^{52}Cr as described above, and can be represented as the area beneath the thin black line in Fig. 1. I_{52Cr} refers to the intensity (cps) measured by the electron multiplier of the background $^{52}Cr^+$, as calculated from the intensity of $^{53}Cr^+$, the non-implanted Cr species of known concentration; and t is the total time of the profile in seconds,

$$F_{52Cr} = \frac{C_{52Cr}\,D\,A_{52Cr+}}{I_{52Cr}\,t}. \tag{3}$$

Each NIST glass was profiled twice, and the fluence was calculated from each of the four profiles. There was no difference observed in the fluence calculated within a single NIST glass material or between the NIST 614 and 612 glasses. The implant fluence was determined to be $2.76 \pm 0.22 \times 10^{13}$ ions/cm^2, a significant deviation from the nominal fluence of 4×10^{13} ions/cm^2. Quoted uncertainties are 2SD in the calculated fluence and incorporate uncertainties in the Cr concentrations of the NIST glass reference materials and the variability of the calculated fluence between the rastered areas; other sources of error (e.g., of crater depth determinations) contribute negligibly to the overall uncertainty.

TABLE II. Results of RSF values derived from the depth profiling of natural carbonate minerals. The error on the RSF value is 2SD. Refer to Table I for additional information about error in Fe and Mn concentrations. Fe and Mn concentrations are reported in mol.% or ppm as μg Mn/g.

Name	RSF	±	Depth (nm)	SD (%)	^{55}Mn (cps)	$A(^{52}Cr^+)$ (counts)	Time (s)	Fe	Mn
Calcite No. 1	1.66	1.5	301	1.0	138	115 472	1637	b.d.	b.d.
Calcite No. 2	1.60	1.5	297	1.7	163	131 794	1612	b.d.	b.d.
MS1317 No. 1	1.03	0.67	302	2.0	462	118 566	1767	b.d	(317)
MS1317 No. 2	1.32	0.86	285	4.0	915	158 026	1761	b.d	(317)
MS1317J No. 1	1.16	0.25	327	1.3	3326	151 971	1470	1.4	0.2
MS1317J No. 2	1.23	0.27	651	0.5	2506	143 986	3470	1.4	0.2
MS1318 No. 1	0.867	0.16	293	0.6	28 369	214 744	1842	8.2	1.1
MS1305 No. 1	0.865	0.3	332	0.7	1976	152 105	1859	0.9	(558)
MS1305 No. 2	0.825	0.29	329	0.8	1965	145 875	1861	0.9	(558)
MS1312 No. 1	0.848	0.07	275	2.6	157 260	181 010	1915	22.8	8.2
MS1312 No. 2	0.927	0.08	315	5.7	105 714	177 507	2387	21.9	6.6

B. Calculation of relative sensitivity factors

The relative sensitivity factor of an implanted natural material can be calculated according to Eq. (4), where C_{55Mn} represents the concentration of ^{55}Mn as determined by EPMA, D represents the depth of the rastered area, A_{52Cr^+} represents the total number of counts of implanted $^{52}Cr^+$ (as defined above), I_{55Mn} represents the measured signal intensity of $^{55}Mn^+$ during the depth profile, F represents the fluence of ^{52}Cr implanted as calculated above, and t represents the total duration of the profile,

$$RSF = \frac{C_{55Mn} D A_{52Cr^+}}{I_{55Mn} F t}. \quad (4)$$

The RSF values for each implanted carbonate, along with the parameters from Eq. (3) used to calculate the RSF, are summarized in Table II. The relationship between the RSF value and the Fe content of the carbonate is shown in Fig. 3. Uncertainties in the derived RSF value incorporate errors in the Mn concentration and the fluence. As the relative uncertainty for the fluence determination is 8% (= 2SD) (quantified empirically from depth profiling of the implanted NIST glasses; see above), the error for the RSF for most carbonates is dominated by the error in the Mn concentration as determined by the EPMA. All repeated measurements of the RSF of carbonate materials are within error of one another. Because the calcite Mn concentration was below the detection limit of the EPMA (120 ppm), a Mn concentration of 100 ppm was used in order to perform the calculation. Therefore, the calcite RSF of 1.63 represents an upper bound and is associated with an error of 100%.

C. Nonlinear variation of relative sensitivity factors

For dolomite samples with $FeCO_3 > 8\%$, the RSF remains constant at 0.88 ± 0.08 (2SD). At lower Fe content, the RSF value is higher, rising to around ~1.1 when $FeCO_3$ approaches zero. This trend is consistent with previous studies of matrix effects in instrumental fractionation for carbonate minerals, which also show that isotope fractionation effects change substantially as small amounts of Fe are added to the carbonate but then become nearly constant once some threshold Fe concentration is reached.[15,16]

D. Discussion

1. Comparison of RSFs with previous work

A previously quantified implanted ankerite (24 and 1.4 mol.% Fe and Mn, respectively) is similar to our MS1312 material, though MS1312 contains significantly more Mn.[8] Despite substantial
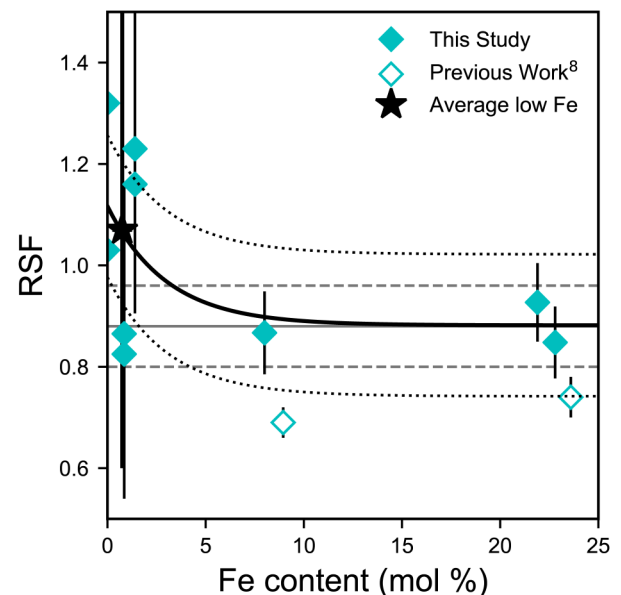

FIG. 3. Mn/Cr relative sensitivity factors of terrestrial carbonate minerals as a function of Fe content. Error bars on the RSF measurements represent 2SD. The average value of all RSF values obtained from low-Fe dolomite is represented by the black star. The gray line represents the average value for high-Fe dolomite analyzed in this study and related errors (2SD). RSF values obtained by Steele et al. are plotted with open symbols for comparison (Ref. 8). The exponential fit (black line) and related errors (dotted black lines, 2SD) were calculated using the curve_fit function from the SciPy Optimization module (Ref. 14).

differences in the analytical conditions between this work and the previous study, the RSF value of 0.888 obtained for MS 1312 is higher than, though similar to, the value determined in the previous work for this similar mineral and is consistent with the overall trend of lower RSF with higher Fe content.[8] Comparison of our MS1318 material (8.2 and 1.1 mol. % Fe and Mn) with a similar ferroan dolomite (8.5 and 0.5 mol. % Fe and Mn) show that the RSF value of 0.867 for MS 1318 is higher than that determined for the previously quantified dolomite, though we note that Steele *et al.* report only the standard error for their study. For comparison with other determinations of the calcite RSF, a nearly pure $CaCO_3$ calcite was also implanted. However, only an upper limit of 120 ppm could be established for the Mn abundance for this material by EPMA. The calcite RSF we calculate assuming a Mn concentration of 100 ppm, though consistent within error with previous calcite RSF determinations of 1.16–1.41,[5–8] is associated with large errors related to poor constraints on the Mn concentration.

2. Uncertainty in Mn concentration

Large errors in the RSF when $FeCO_3 < 2\%$ are due to challenges in quantifying the Mn concentration by EPMA. In these low-Mn carbonates, Mn is heterogeneous on the order of a few 100 ppm at the spatial scale of our analyses. At low Mn concentration, this heterogeneity combined with a ~120 ppm detection limit of EPMA leads to substantial uncertainty in the calculated RSF. Although this might appear to be a significant problem in quantifying systematics of the matrix effect, in practice it is not very important. Meteoritic dolomite typically incorporates $MnCO_3 > 2$ mol. % and $FeCO_3 > 4$ mol. %.[4,17] Therefore, we do not expect large errors due to poor Mn (or Fe) quantification in natural meteoritic carbonate.

3. Change of RSF with depth

In a previous study by Doyle *et al.*,[18] the Mn/Cr RSF was shown to vary with depth during the analysis of olivine, a mineral that naturally incorporates trace amounts of Cr. These analyses were performed in the "spot mode," as is typical for ^{53}Mn-^{53}Cr geochemical analyses. The craters produced by Doyle *et al.* were 3 and 5 μm in diameter with a significantly greater depth/diameter ratio than those were produced in our study, where the primary beam was rastered over a $50 \times 50 \, \mu m^2$ area resulting in shallow (<1 μm deep) craters. Doyle *et al.* further found that the magnitude of the RSF variation changed depending upon the Fe content of the olivine: for an olivine of low Fe content (Fa_{10}), the value of the RSF increased by 10% over the course of the analysis, whereas for an olivine of higher Fe content (Fa_{34}), it increased only by only 4%. Because we have implanted Cr into the target, we cannot characterize any possible depth-dependent RSF variations for carbonates using the same method as has been applied to olivine.

Matrix effects are challenging to predict and model. As an example, in stable isotope analyses of $\delta^{18}O$ in carbonates of varying Fe content, increasing Fe content results in a bias toward higher values of $\delta^{18}O$.[16] In contrast, $\delta^{18}O$ in olivine would show the opposite relationship with the increasing Fe content.[19] Therefore, we do not make a quantitative attempt to use the

variation in RSF during the sputtering of olivine to predict the behavior of the carbonate RSF.

In this work, we show that the RSF decreases from ~1.1 at 0 mol. % Fe to 0.88 at 8–20 mol. % Fe for an overall change of 19%. The magnitude of this effect is larger than the depth-induced RSF change observed in olivine, although we do not know how carbonate would compare with olivine in terms of the degree of RSF variation with depth. As we continue to develop this method, we plan to conduct test analyses on implanted standards using smaller raster sizes (different crater aspect ratios) to assess the variability of the RSF in these different materials.

4. Effect of incorrect RSF usage

To illustrate the importance of selecting the appropriate RSF value on the determination of initial $^{53}Mn/^{55}Mn$ in a carbonate, we consider a fictional dolomite with an inferred $^{53}Mn/^{55}Mn$ ratio of 4.00×10^{-6} before correction for matrix effects. Since the inferred $^{53}Mn/^{55}Mn$ ratio is inversely proportional to $^{55}Mn/^{52}Cr$, a smaller RSF value would result in a smaller true $^{55}Mn/^{52}Cr$ [Eq. (2)] and thus a higher $^{53}Mn/^{55}Mn$. If this hypothetical carbonate was corrected using an RSF value of 1.1 appropriate for a low-Fe dolomite, it would correspond to a $^{53}Mn/^{55}Mn$ ratio of 3.64×10^{-6} for an age, as calculated by Eq. (1), of 3.9 Myr after the birth of the solar system. On the other hand, if an RSF value of 0.88 is used as would be more appropriate for a high-Fe dolomite, the inferred $^{53}Mn/^{55}Mn$ ratio would be 4.55×10^{-6} corresponding to an age of 2.1 Myr after the birth of the solar system—a systematic difference of 1.8 Myr. Because the ^{53}Mn-^{53}Cr chronometer is used only within the first 15 Myr of the solar system's history, a systematic error of 1.8 Myr would represent a significant change to the interpretation of the chronology of hydrothermal alteration in the parent asteroid of a given meteorite.

IV. SUMMARY AND CONCLUSIONS

We used ion implantation of a suite of terrestrial dolomite reference materials to show that the relative sensitivity factor for dolomite with 8%–20% $FeCO_3$ is 0.88 ± 0.04, consistent with previous estimates made for carbonates containing higher $FeCO_3$. At low Fe and Mn content, the RSF is ~1, although this value is associated with significant error due to uncertainties in the Mn concentration.

REFERENCES

[1] A. M. Davis and K. D. McKeegan, in *Treatise on Geochemistry*, 2nd ed., edited by H. D. Holland and K. K. Turekian (Elsevier, Oxford, 2014), pp. 361–395.

[2] D. P. Glavin, A. Kubny, E. Jagoutz, and G. W. Lugmair, Meteorit. Planet. Sci. **39**, 693 (2004).

[3] G. A. Brennecka and M. Wadhwa, Proc. Natl. Acad. Sci. U.S.A. **109**, 9299 (2012).

[4] S. de Leuw, A. E. Rubin, A. K. Schmitt, and J. T. Wasson, Geochim. Cosmochim. Acta **73**, 7433 (2009).

[5] W. Fujiya, N. Sugiura, H. Hotta, K. Ichimura, and Y. Sano, Nat. Commun. **3**, 627 (2012).

[6] W. Fujiya, N. Sugiura, Y. Sano, and H. Hiyagon, Earth Planet. Sci. Lett. **362**, 130 (2013).

[7] C. E. Jilly, G. R. Huss, A. N. Krot, K. Nagashima, Q.-Z. Yin, and N. Sugiura, Meteorit. Planet. Sci. **49**, 2104 (2014).

[8] R. C. J. Steele, V. S. Heber, and K. D. McKeegan, Geochim. Cosmochim. Acta **201**, 245 (2017).

[9] N. Sugiura, K. Ichimura, W. Fujiya, and N. Takahata, Geochem. J. **44**, e11–e16 (2010).

[10] E. Usdowski, *Dolomites* (John Wiley & Sons, Ltd, Hoboken, NJ, 2009), pp. 345–360.

[11] D. S. Burnett *et al.*, Geostand. Geoanal. Res. **39**, 265 (2015).

[12] K. P. Jochum *et al.*, J. Geostand. Geoanal. Res. **35**, 397 (2011).

[13] J. F. Ziegler, M. D. Ziegler, and J. P. Biersack, Nucl. Instrum. Met. B **268**, 1818 (2010).

[14] P. Virtanen *et al.*, Nat. Met. **17**, 261 (2020).

[15] M. G. Śliwiński, K. Kitajima, R. Kozdon, M. J. Spicuzza, J. H. Fournelle, A. Denny, and J. W. Valley, Geostand. Geoanal. Res. **40**, 157 (2016).

[16] M. G. Śliwiński, K. Kitajima, R. Kozdon, M. J. Spicuzza, J. H. Fournelle, A. Denny, and J. W. Valley, Geostand. Geoanal. Res. **40**, 173 (2016).

[17] M. Tyra, A. Brearley, and Y. Guan, Geochim. Cosmochim. Acta **175**, 195 (2016).

[18] P. M. Doyle, K. Jogo, K. Nagashima, G. R. Huss, and A. N. Krot, Geochim. Cosmochim. Acta **174**, 102 (2016).

[19] J. Isa, I. E. Kohl, M.-C. Liu, J. T. Wasson, E. D. Young, and K. D. McKeegan, Chem. Geol. **458**, 14 (2017).

[20] See supplementary material at https://doi.org/10.1116/6.0000111 for extended methods, figures, and data tables.